ELSEVIER

Applied Catalysis A: General 177 (1999) 53–68

APPLIED CATALYSIS A: GENERAL

Structure and catalytic activity of $La_{1-x}FeO_3$ system (x=0.00, 0.05, 0.10, 0.15, 0.20, 0.25, 0.35) for the NO+CO reaction

V.C. Belessi[a], P.N. Trikalitis[a], A.K. Ladavos[a], T.V. Bakas[b], P.J. Pomonis[a,*]

[a]*Department of Chemistry, University of Ioannina, Ioannina 45332, Greece*
[b]*Department of Physics, University of Ioannina, Ioannina 45332, Greece*

Received 10 November 1997; received in revised form 15 July 1998; accepted 20 July 1998

Abstract

Solids of the nominal formula $La_{1-x}FeO_3$ where x=0.00, 0.05, 0.10, 0.15, 0.20, 0.25, 0.35, and containing only the perovskite (small x) and the perovskite plus Fe_2O_3 crystal phases (large X) were examined in the catalytic reaction of (NO+CO). The solids were prepared by heating at T=1000°C under ~10^{-5} Torr vacuum and showed appreciable catalytic activity at temperatures from 280°C to 480°C when SV is ~300 h^{-1}. XRD analysis and Rietveld refinement showed that for x=0.00 and 0.05 only the perovskite phase is apparent. For $x\geq$0.10 an additional crystal phase of Fe_2O_3 appears which increases with x up to a maximum of 4.1% at x=0.35. Moessbauer examination indicated that iron exists in the perovskite structure at x=0.00 and 0.05 but for $x\geq$0.10 the extra-perovskite Fe^{3+} increases proportional to the parameter x of the solids $La_{1-x}FeO_3$ and reaches 43% at x=0.35. These results are explained assuming that in the catalyst particles with $x\geq$0.10 a Fe_2O_3 core of increasing size is covered by a $LaFeO_3$ shell. The sample $LaFeO_3$ showed lower catalytic activity for the NO+CO reaction than the rest of $La_{1-x}FeO_3$ solids. The Arrhenius plots showed two distinct regions of activity one at low temperature with high apparent activation energies and another at high temperature with lower apparent activation barriers. At low temperatures the low activity at x=0.00 is related to high apparent activation energies while for $x\geq$0.05 the opposite is true. A detailed scrutinization of the apparent activation energies resulted in an estimation of the heats of adsorption of NO on $LaFeO_3$ and $La_{1-x}FeO_3$. The reaction of NO+CO also resulted in small amounts of N_2O which showed a maximum at ~320°C. The dependence of N_2O production and elimination on the temperature made it possible to determine the activation energies of its formation as well as the heat of desorption of nitrogen from the catalyst surface. The catalytic activity of the solids is destroyed if they are heated under atmospheric conditions.

Keywords: Perovskite; La–Fe–O; Catalytic decomposition; Nitrogen monoxide; Rietveld; Moessbauer

1. Introduction

The reaction between NO and CO has attracted the interest of many research groups since both reactants exist in effluent gases of both mobile and immobile sources and their interconversion would solve a lot of environmental problems. For this reason the reaction has been studied extensively on noble metals, mainly in motor industry research facilities [1–11] as well as on perovskite ceramic solids, mainly in university laboratories [12–19]. We notice that perovskites show generally poorer performance as compared to noble metals. Nevertheless, there are cases where their activity is comparable and a number of patents from

*Corresponding author.

0926-860X/99/$ – see front matter
PII: S0926-860X(98)00256-7

various industries cover the use of perovskites as depolluting catalysts [20–22]. These ceramic materials are often nick-named *chemical chameleons* because their physicochemical properties alter dramatically by substitution or by introduction of heterocations of different valences into their structure. Thus compounds of the general formula $A^{3+}_{1-x}C^{2+}_{x}B^{3+}_{1-x}B^{4+}_{x}O_3$ or $A^{3+}_{1-x}C^{4+}_{x}B^{3+}_{1-x}B^{2+}_{x}O_3$ exhibit mixed valences and show interesting magnetic, electric, surface and catalytic properties [19,23–28]. The reason for such a behaviour is that the mixed valencies are not thermodynamically well stabilized and therefore are easily intertransformed from an initial to a final configuration, and vice versa, with a small energy push. A particular subject which has been little searched relevant to perovskites ABO_3 is the influence of the lack of stoichiometry on their surface and catalytic properties. Voorhoeve and co-workers [29] investigated the influence of vacancies of metal A on the catalytic activity of perovskites A_{1-x} Ø BO_3 for the reduction of NO by CO and H_2 and they found that the energy of the metal–oxygen bond is important for the process. Also in a recent work [30] the influence of the non-stoichiometry was studied for the system Sr_xTiO_{2+x} but the interest of the authors was focused on the surface basicity rather than on its catalytic action. The purpose of the present article is to study the shift from stoichiometry of the perovskites $La_{1-x}FeO_3$ (x=0.00, 0.05, 0.10, 0.15, 0.20, 0.25 and 0.35) on their catalytic performance for the NO+CO reaction. A relevant question is the mechanism of the reaction on such systems and what kind of alternations is suffered on the modified, non-stoichiometric solids.

2. Experimental

2.1. Preparation of materials

The materials $La_{1-x}FeO_3$ with x=0.00, 0.05, 0.10, 0.15, 0.20, 0.25, 0.35 were prepared via the so-called ceramic method as follows: Calculated amounts of La_2O_3 (Aldrich) and Fe_2O_3 (Ventron) were mixed for 2 h in a planetary mill (Fritsch puluerisette 5) in a ZrO_2 vessel. Then the mixture was pressed into pellets under 6 ton pressure and heated at T=1000°C under vacuum (10^{-5} Torr) for 6 h, followed by grinding, pelletization and heating again under exactly the same conditions at 1000°C for another 6 h and grinding finally in an agate mortar. The obtained materials with some of their properties are shown in Table 1.

2.2. Characterization of the solids

XRD analysis. The crystal structure of the prepared materials was determined by XRD analysis using a Siemens Diffract 500 system employing Cu K_α radiation (λ=1.5418 Å).

Surface area measurements. The specific surface area of the solids was checked by N_2 porosimetry (BET) at T=77 K using a single point Carlo Erba Sorpty 1750 and a multi-point Fisons Sorpty 1900 System.

Moessbauer studies. ^{57}Fe Moessbauer spectra were obtained for all samples at 300 and 20 K, using a closed loop refrigerator system. A constant acceleration spectrometer was used to move a ^{57}Co(Rh) source kept at 300 K. The spectrometer was calibrated with

Table 1
Prepared solids, heating conditions, detected crystal phases (XRD/Rietveld and Moessbauer) and the found apparent activation energies for the NO and CO conversion at low and high temperatures

Solids	T (°C)/time (h)	Crystal phases (%)				E_a (kJ/mol)					
		Rietveld		Moessbauer		NO		CO		N_2O	
		$LaFeO_3$	Fe_2O_3	$LaFeO_3$	Fe_2O_3	Low T	High T	Low T	High T	Low T	High T
$LaFeO_3$	1000/6+6	100	–	100	–	59.3	8.2	109.0	19.6	29.2	−10.3
$La_{0.95}FeO_3$	1000/6+6	100	–	100	–	40.6	13.3	47.2	13.0	–	−3.84
$La_{0.9}FeO_3$	1000/6+6	98.8	1.2	91	9	38.2	14.2	48.8	14.5	–	−36.7
$La_{0.85}FeO_3$	1000/6+6	97.7	2.3	81	19	48.5	15.7	55	18.2	2.3	−27.1
$La_{0.8}FeO_3$	1000/6+6	97.4	2.5	76	24	48.5	14.3	62.1	15.3	4.5	−53.9
$La_{0.75}FeO_3$	1000/6+6	96.7	3.3	69	31	36.9	11.8	48.7	13.9	14.1	−31.9
$La_{0.65}FeO_3$	1000/6+6	95.9	4.1	57	43	40.5	13.9	51.0	18.1	1.8	−46.4

α-Fe and isomer shift values are given relative to this. The experimental data were fitted by a least squares computer minimization using a sum of spectral components characterizing different iron phases [31].

2.3. Catalytic activity

The catalytic activity tests of solids $La_{1-x}FeO_3$ for the NO+CO reaction was carried out in a bench scale tubular plug flow reactor (PFR) under atmospheric pressure. Briefly a mixture of reactants in the ratio NO:CO:He=2:2:96 at a total flow of 90 ml/min was passed through the catalyst bed containing 250 mg of the catalyst. Under those conditions the space velocity was calculated to be around 280 ml/ml h. The system was heated externally via a tubular furnace, regulated by a SUR BERLIN controller, via a thermocouple in touch with the catalyst bed, within ±2°C. Analysis of the reactants and products was carried out chromatographically using a Carlo Erba chromatograph equipped with a TCD with He as carrier gas and connected to a PC for data acquisition. A 10-port valve controlled via the PC, enables sampling of 1 cm^3 of reactants and products for analysis using a two-column system, Porapac Q and Molecular Sieve 13X, similar to that described in [16]. The catalysts were tested in the temperature region of 300–500°C and from the data obtained the degrees of conversion and reaction rates were calculated.

3. Results

3.1. Surface area

The specific surface area of the ceramic solids was found to be less than 2–3 m^2/g. So practically it was not taken into account in the calculation of the reaction rates.

3.2. The crystal composition of the $La_{1-x}FeO_3$ solids using Rietveld analysis of the XRD data

The X-ray diffractograms obtained from the solids $La_{1-x}FeO_3$ are shown in Fig. 1 and include only the crystal phases of $LaFeO_3$ and Fe_2O_3.

Using as starting models these two crystal phases, a Rietveld refinement of the obtained XRD data was made according to the methodology developed in [32–35] and using a relevant computer program for quantitative phase analysis of multicomponent mixtures [36]. The data used for the refinement of each phase were taken from a standard reference handbook [37]. The refinement parameters accordingly for all the above phases include scale factors, background coefficients, peak width, profile parameters, occupancy factors and cell dimensions and were treated as described in [36]. The results of the simulations obtained between the experimental and the Rietveld procedure are shown in Fig. 2.

We observe that the simulations are quite satisfactory as seen by the small values of ΔY deviations shown in each case. The determined percentages of the two crystal phases, $LaFeO_3$ and Fe_2O_3, contributing to the simulated XRD spectra are included in Table 1. We observe that the amount of Fe_2O_3 remains low between 1% and 4% and does not exceed the 4.1% value even at the solid $La_{0.65}FeO_3$. We draw attention to the fact that the crystal composition of the solids determined by this method is referred only to the depth where the X-rays can penetrate the ground solid and cannot provide information for the bulk of it.

3.3. The Moessbauer studies

The Moessbauer spectra of all samples taken at room temperature have the same spectrum profile. The spectra consist of one six line pattern with hyperfine parameters of $LaFeO_3$ [32]. No sign of a second magnetic or paramagnetic component is detectable as is clearly visible in Fig. 3.

The spectra at 20 K of the samples with $x>0.1$ consist of two magnetically splitted components one for the $LaFeO_3$ and one for the Fe_2O_3, typical results are shown in Fig. 4. The hyperfine parameters deduced after computer analysis for all spectra at 20 K are shown in Table 2. From the parameters of the spectra at 20 K it is obvious that there is an almost one-to-one correspondence between the departure from the stoichiometry of the solids $La_{1-x}FeO_3$, as determined by the x values, and the % Fe_2O_3-phase evaluated from the computer analysis (see also Table 1). There was no difference in the Moessbauer parameters at room temperature or at 20 K for the samples after their use for the interconversion between NO and CO. This

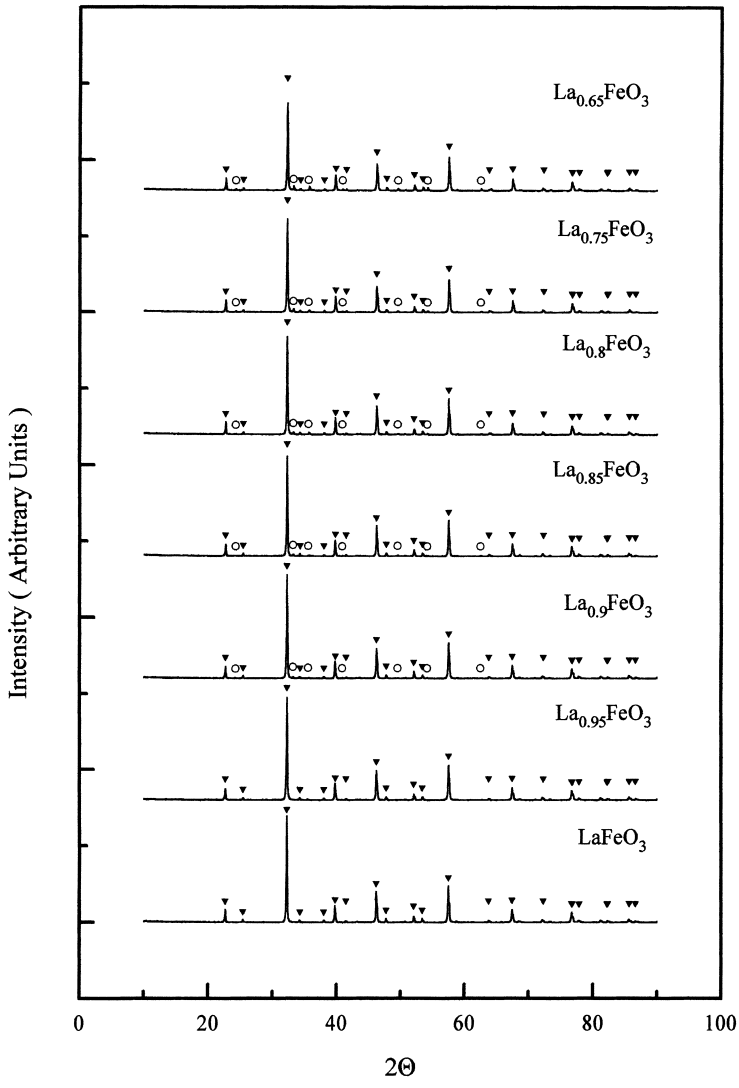

Fig. 1. XRD analysis of the solids $La_{1-x}FeO_3$: (▼) Perovskite; (○) Fe_2O_3.

means that there is no change in the environment of Fe after this reaction detectable by Moessbauer spectroscopy.

3.4. Catalytic activity

The solids $La_{1-x}FeO_3$ were active for the interconversion of NO and CO between ≈280°C and 480°C. The temperature profiles for the % conversion of both reactants are shown in Fig. 4. The products of the reaction were N_2, CO_2 and N_2O. From Fig. 4 we observe that at low temperatures the conversion of NO is higher as compared to CO while as the temperature increases the two reactants tend to react in equal degrees of conversion. For comparison the data on a pure sample of Fe_2O_3 prepared under similar conditions are also included.

The excess of the NO conversion as compared to that of CO at low temperatures is related to the production of N_2O, also shown in Fig. 4 with dashed line in arbitrary units. The production of N_2O shows a maximum which varies depending on the sample and as the temperature increases its production decreases. In Fig. 5 the production of N_2O is related to the

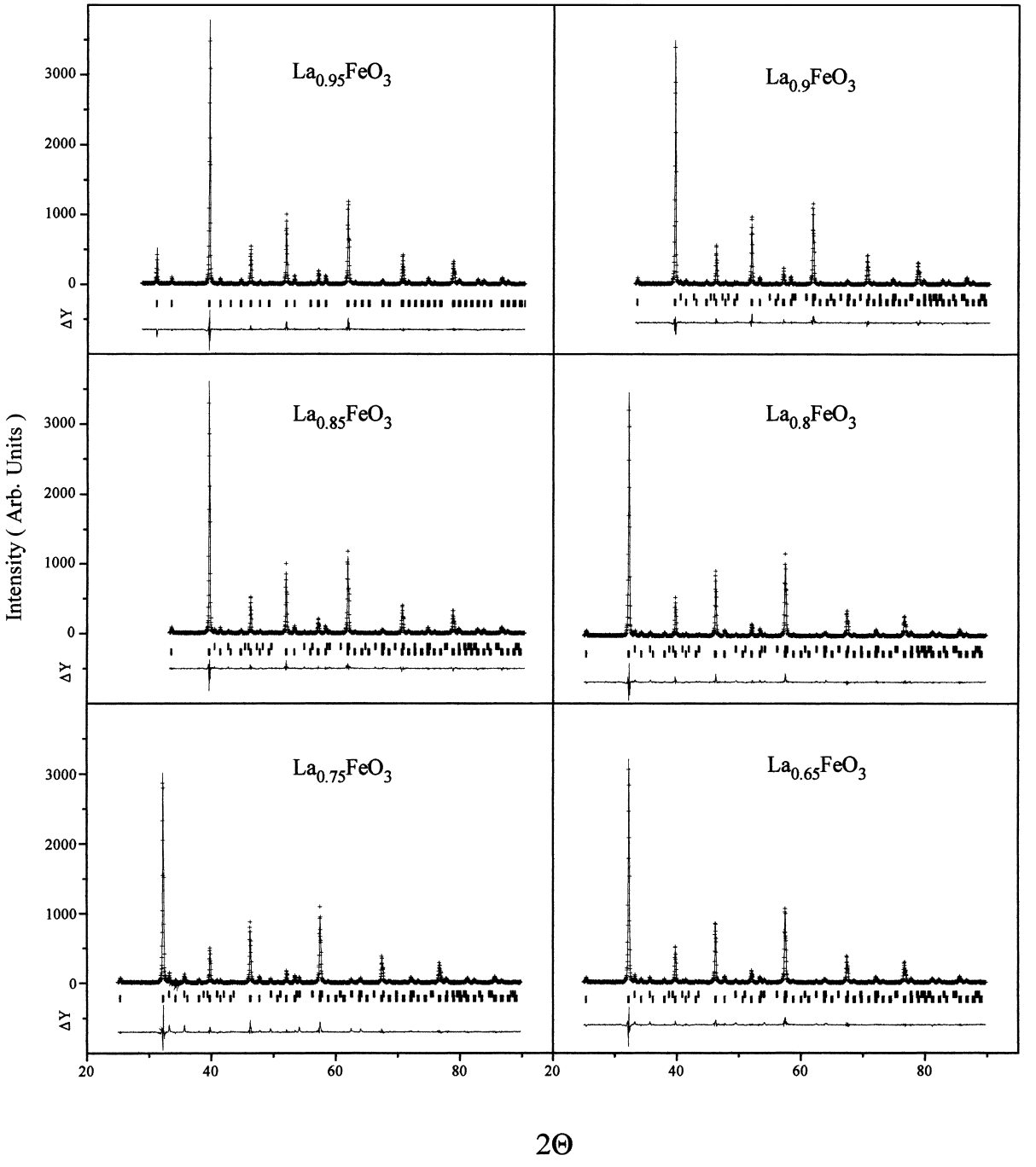

Fig. 2. Results from the Rietveld analysis for the $La_{1-x}FeO_3$ solids.

difference between the NO and CO conversion and it is also shown as a function of the parameter x of the $La_{1-x}FeO_3$ solids.

In the same figure the reaction rate for the NO and CO conversion (mol/g s) is shown vs. the nominal parameter x of the $La_{1-x}FeO_3$ solids. In Fig. 6 the ratio

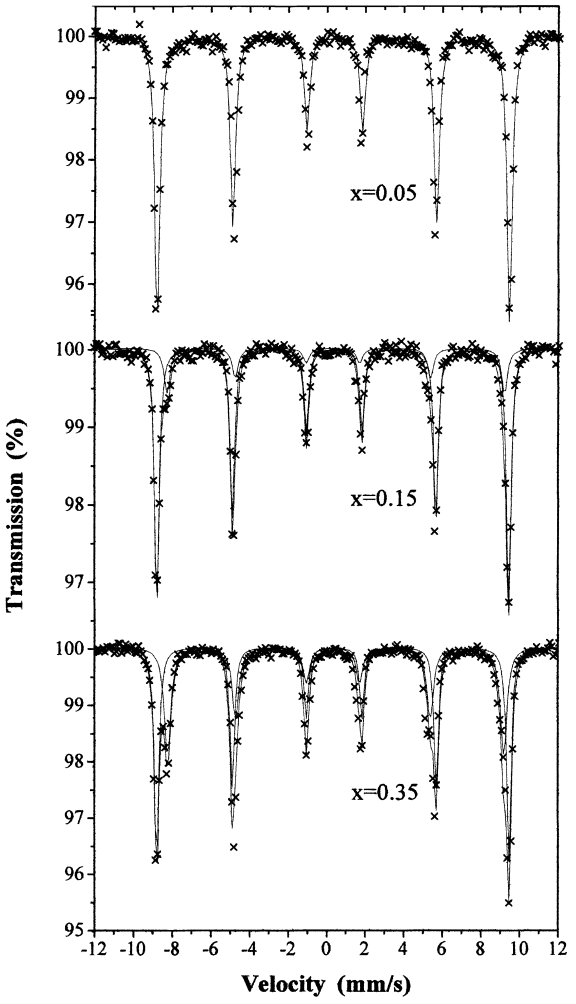

Fig. 3. Typical Moessbauer spectra of the indicated solids.

of the degrees of conversion X_{NO}/X_{CO} as well as the variation of the ratio of the products CO_2/N_2+N_2O are shown as a function of temperature.

Finally, in Fig. 7 the Arrhenius lines for the NO conversion have been drawn from plots of $\ln R$ vs. $1000/T$. We observe that there are two distinct and clearly differentiated regions of the slope: One at low and the other at high temperatures. From those slopes the corresponding apparent activation energies have been calculated and cited in Table 1, separately for the low temperature (LT) and the high temperature (HT) regions. Exactly similar plots done for CO conversion led to the calculation of the corresponding apparent activation energies at LT and HT. The corresponding values are also given in Table 1.

4. Discussion

4.1. Activity patterns of the solids

The reaction between NO and CO on various perovskite solids has been shown that proceeds via two distinct routes which are differentiated according to temperature [16–20,24,38–42]

$$\text{Route 1}: \quad 2NO + 2CO \rightarrow N_2 + 2CO_2 \qquad (1)$$

This route usually takes place at high reaction temperatures and the ratio of the degrees of conversion of reactants NO and CO equals unity ($X_{NO}/X_{CO}=1$), while the ratio of the products equals 2 (moles CO_2/moles N_2O or moles CO_2/moles $[N_2O+N_2]=2$).

Table 2
Moessbauer hyperfine parameters at 20 K

Sample x	δ_{Fe}[a] (mm/s)	ΔEq[a] (mm/s)	H[b] (T)	Area[c] (%)	δ_{Fe}[a] (mm/s)	ΔEq[a] (mm/s)	H[b] (T)	Area[c] (%)
0.00	0.49	−0.06	56.7	100				
0.05	0.49	−0.06	56.7	100				
0.10	0.49	−0.06	56.7	91	0.44	0.09	53.2	9
0.15	0.48	−0.06	56.6	81	0.51	0.15	54.3	19
0.20	0.49	−0.06	56.6	76	0.54	0.20	54.6	24
0.25	0.49	−0.06	56.7	69	0.55	0.19	54.3	31
0.35	0.49	−0.06	56.7	57	0.52	0.19	54.1	43

[a]Relative error ±0.02.
[b]Relative error ±0.2.
[c]Relative error ±2.

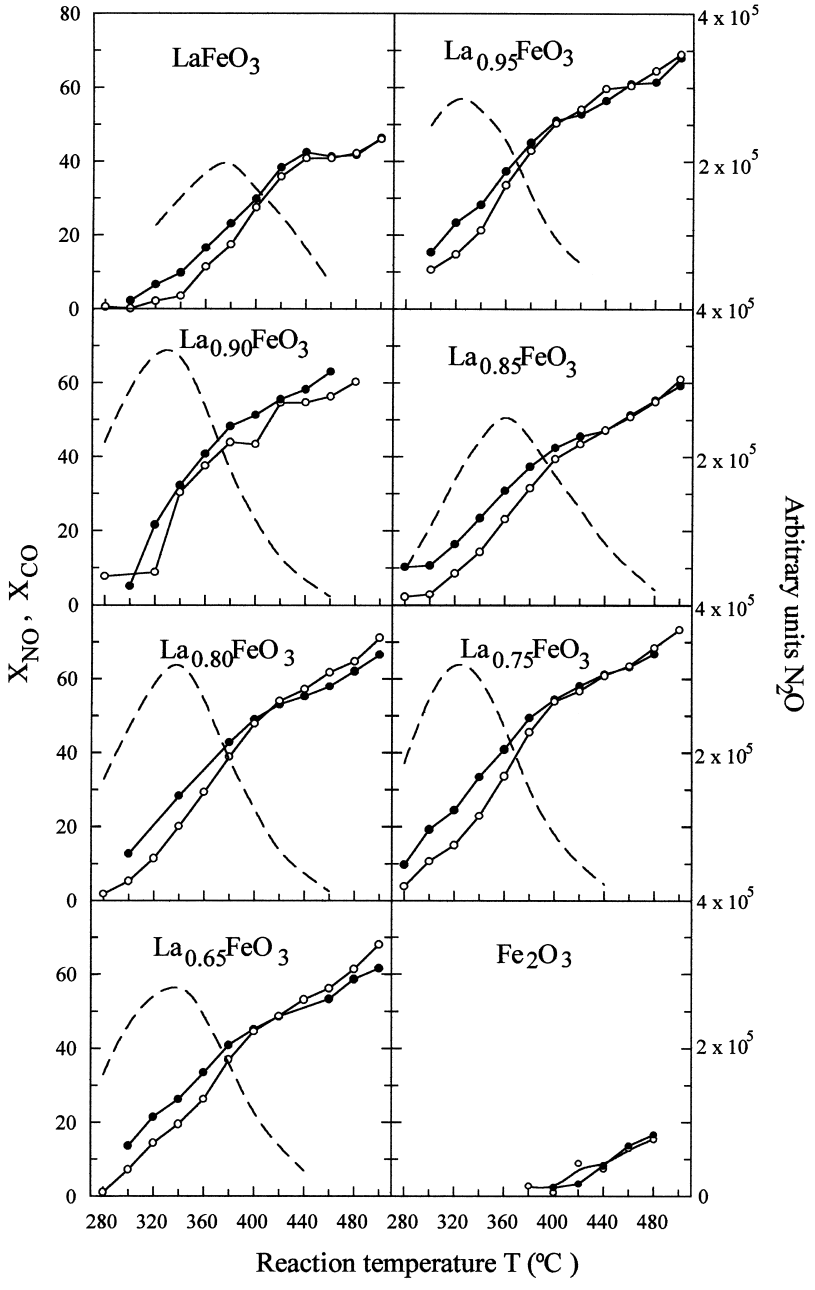

Fig. 4. Temperature profiles for NO (●) and CO (○) conversion and arbitrary units of N_2O production (dashed lines) on the $La_{1-x}FeO_3$ solids. The temperature profiles for NO and CO conversion on Fe_2O_3 are also included for comparison.

Route 2 : $2NO + CO \rightarrow N_2O + CO_2$

$\rightarrow N_2 + \frac{1}{2}O_2 + CO_2$ (2)

This route usually takes place at a low reaction temperature and the ratio of the degrees of conversion of reactants NO and CO equals 2 (X_{NO}/X_{CO}=2), while the ratio of products equals unity (moles CO_2/moles N_2O or moles CO_2/moles [N_2O+N_2]=1).

Therefore plots of X_{NO}/X_{CO} vs. temperature as well as moles CO_2/moles N_2O+N_2 vs. temperature provide

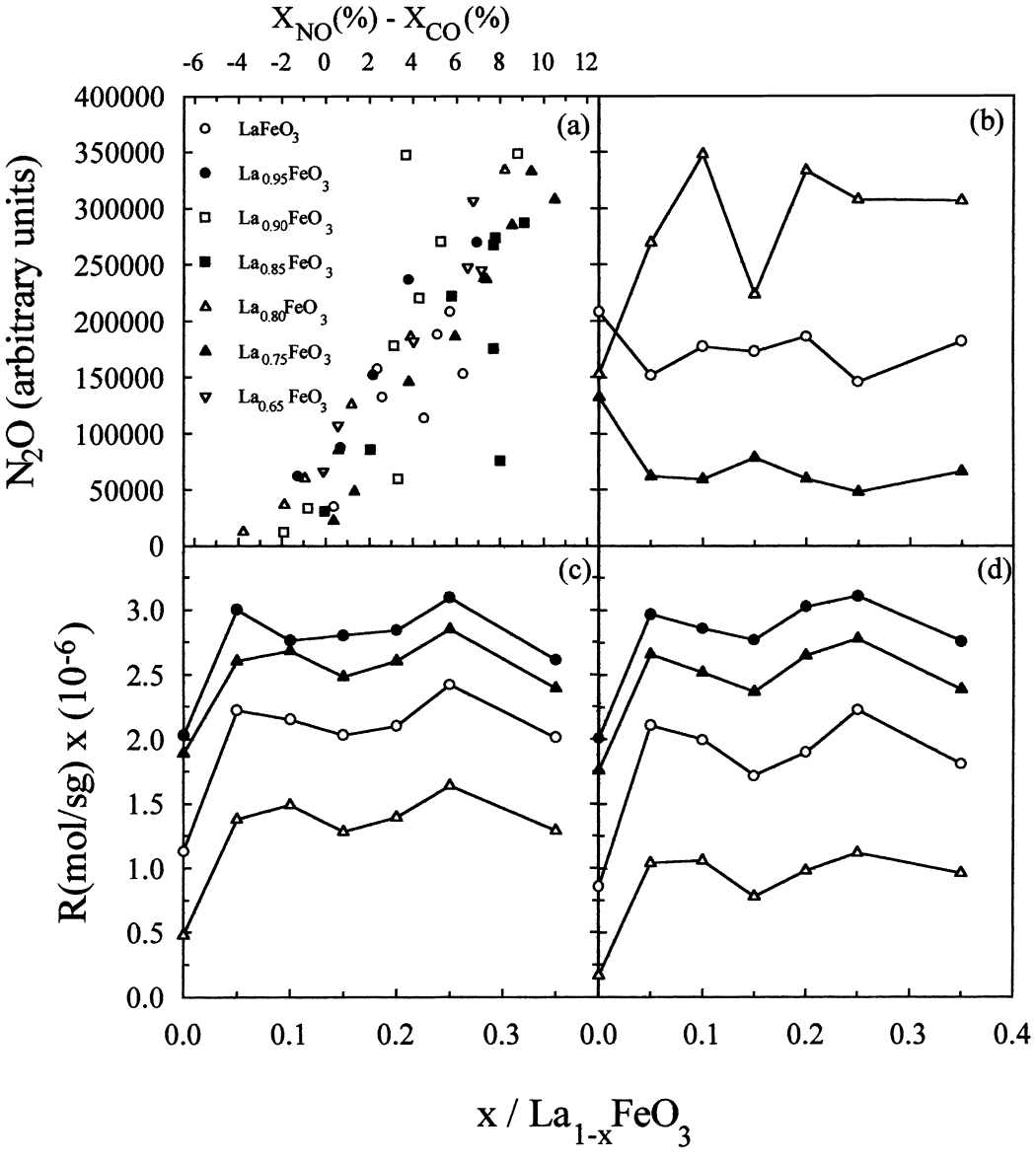

Fig. 5. (a) The relationship between the production of N_2O (arbitrary units) and the difference in the % conversion of NO and CO, (b) the production of N_2O as a function of x at temperatures 340°C (△), 380°C (○), 420°C (▲) and the variation of the rate of NO reduction (c) and CO oxidation (d) vs. x at 340°C (△), 380°C (○), 420°C (▲) and 460°C (●).

an easy way to probe the gradual transition from route 2 to route 1. This is done in Fig. 6, from which this route transition can be clearly traced. These alternations in the reaction stoichiometry are the result of alternation of the reaction mechanism [38] and can be further probed by calculating the apparent activation energies of the reaction which appear to be differentiated in the LT and HT region. This is done in Fig. 8 and the values of $E_{\text{app. NO}}$ and $E_{\text{app. CO}}$ found at LT and HT together with their differences are shown in Fig. 8 as a function of the parameter x of the solids $La_{1-x}FeO_3$.

From this figure as well as from Fig. 5 which show the reaction rate vs. x, we observe that there are two

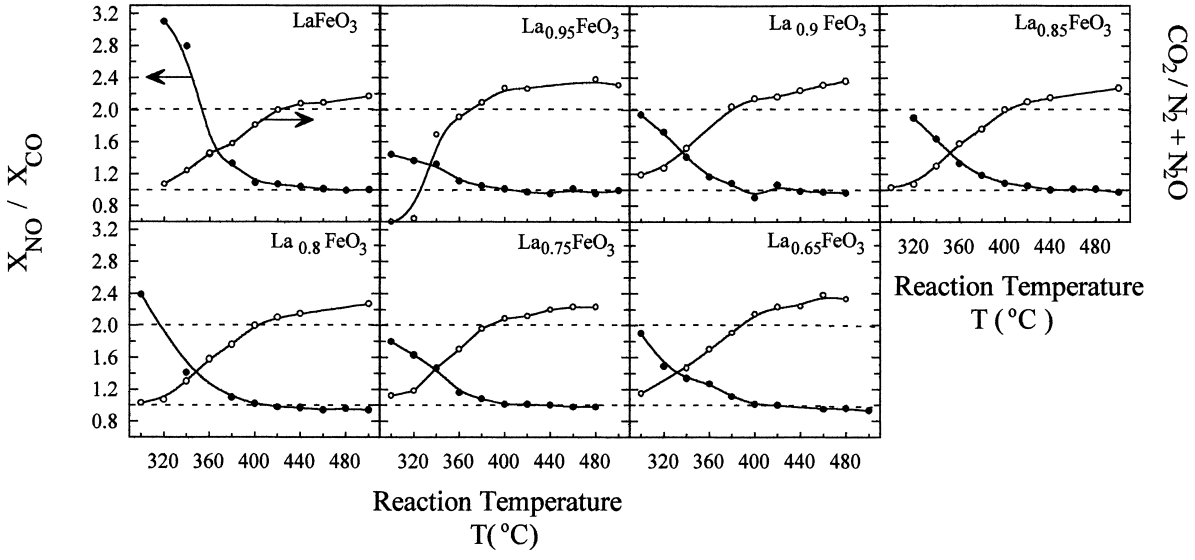

Fig. 6. Ratios of the degrees of conversion X_{NO}/X_{CO} and of the reaction products CO_2/N_2+N_2O vs. reaction temperature.

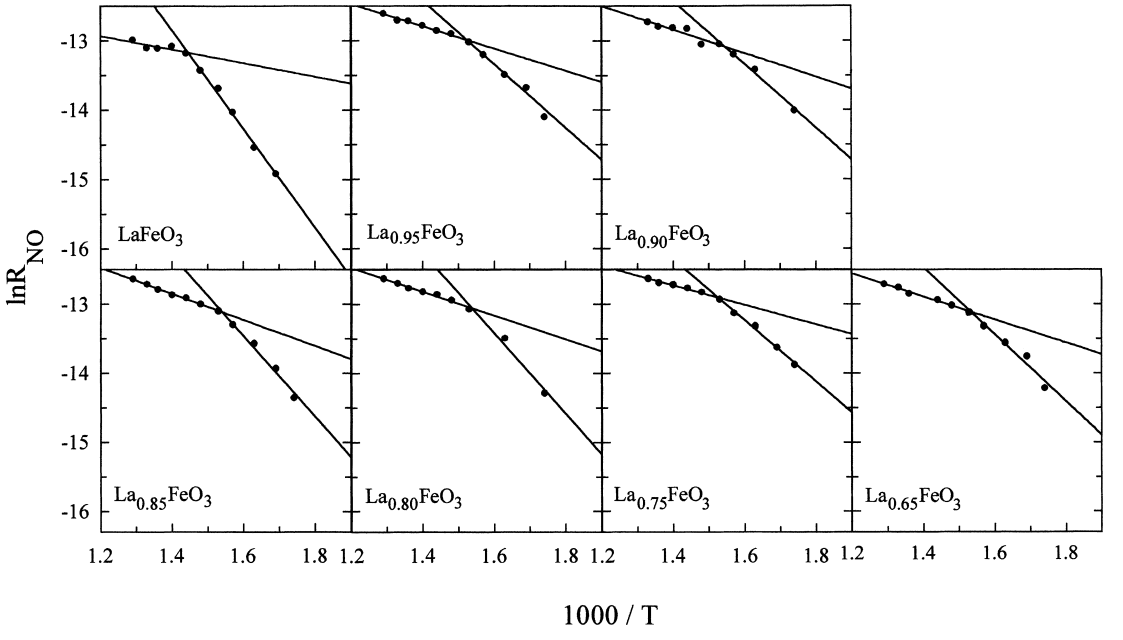

Fig. 7. Arrhenius plots for the NO conversion.

reaction domains: One for the sample $LaFeO_3$ (x=0) which show low activity (Fig. 5) and relative high E_{app} (Fig. 8(a)) and another for the rest of the samples $La_{1-x}FeO_3$ (x=0.05–0.35) in which the activity is much increased (see Fig. 5) while the apparent activation energies are much lower for both NO and CO conversion (see Fig. 8(a)). We emphasize that the lower E_{app} observed at high temperatures, as compared to that in low ones, cannot be due to either external or internal diffusion limitations since in the

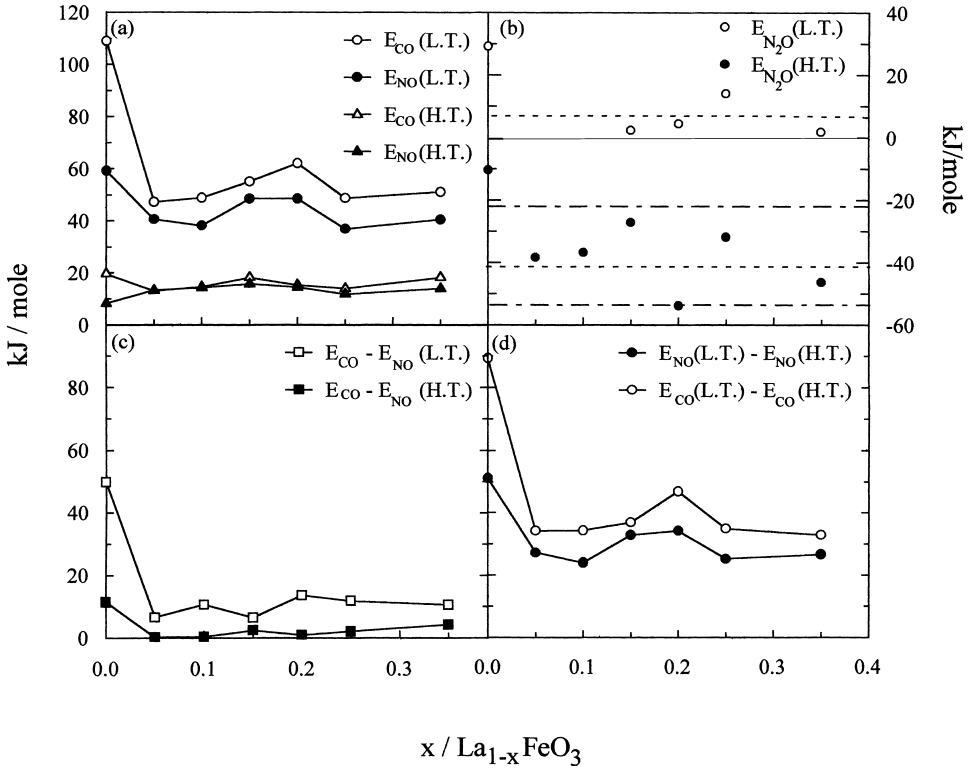

Fig. 8. (a) Variation of the apparent activation energies for NO and CO conversion at the low (LT) and high (HT) reaction temperature regions; (b) the activation parameters for the N_2O formation (LT) and elimination (HT); (c) the differences $E_{NO}-E_{CO}$(HT) and $E_{CO}-E_{NO}$(LT); and (d) E_{NO}(LT)$-E_{NO}$(HT) and E_{CO}(LT)$-E_{CO}$(HT) vs. x in $La_{1-x}FeO_3$.

first case the change of the slope in the Arrhenius plots would be gradual and not sharp as in Fig. 7, while the second case necessitates extensive porosity which is totally lacking in our ceramic solids as concluded by their low ssa ($\leq$3 m^2/g). Therefore the only reason which can explain this drastic change of E_{app} is an alternation of reaction mechanism. These results lead to the following phenomenological explanation for the activity pattern of the $La_{1-x}FeO_3$: Solid $LaFeO_3$ having a stoichiometric perovskite structure, as shown by the XRD/Rietveld analysis as well by the Moessbauer results, shows low activity a fact due to high activation energy of the reaction. But as soon as we depart from stoichiometry (x=0.05) the catalytic activity, as measured by the reaction rate, is nearly doubled and it does not alter significantly as the departure from stoichiometry increases to $La_{0.65}FeO_3$. This increased activity is accompanied by, or rather resulted from, low apparent activation energies. The almost steady reaction rates and activation energies in the whole region $0.05\leq x\leq 0.35$ is due to the fact that the excess of iron in the solid particles does not remain on their surface in Fe_2O_3 form, as exemplified by the lack of any relevant signals in the XRD data (see Table 1). On the contrary, the excess of iron exists in the form of Fe_2O_3 in the inner part of the solid particles as shown by the Moessbauer spectroscopy (Table 1). So the most active phase appears to be the one with a slight lack of stoichiometry $La_{0.95}FeO_3$ which seems to be the outer shell part of the solid particles. It is not clear what would happen if a non-stoichiometric solid, let us say $La_{0.90}FeO_3$, with real lack of stoichiometry 10% was possible to be prepared. In the present case such a solid was not possible to be prepared and it is not clear if this can be done. Nevertheless, the present results hint perhaps to a rule for similar perovskites ABO_3: A lack of stoichiometry of $\sim$5% in the A cation leads to a very substantial increase of the overall activity. It is

worth noticing that the tested solids lose their activity to a very substantial degree when they are heated for 2–3 h under atmospheric conditions. So it seems that a critical parameter for the increased activity is the preparation under decreased pressure.

4.2. Variation of apparent activation energies

As noticed above the alternation from route 2 to route 1, as the temperature of the reaction increases, can only be attributed to an alternation of the reaction mechanism, resulting from the differentiation of the relative enthalpies of adsorption of NO, CO and O on the catalyst surface [38] which influences the apparent activation energies of the reaction. These alternations of the apparent activation energies are clear in Figs. 7 and 8 and Table 1. There are three critical points to draw attention relative to these results:

1. The apparent activation energies appear systematically lower at HT as compared to LT, for both the NO and CO conversion.
2. The apparent activation energies for the CO conversion are systematically higher as compared to that of NO (Fig. 8). This is more apparent at LT where the difference reaches ~10 kJ/mol and less so at HT where $E_{\text{app. CO}} \sim E_{\text{app. NO}}$.
3. The change of the slope in the Arrhenius plots (Fig. 7) corresponding to the change of the apparent activation energies and signalling a transition of the reaction mechanism is well defined in a short range of temperature.

All the above 1–3 points are not to be taken for granted for all perovskitic materials: Thus for the system $La_{2-x}Sr_xNiO_{4-\delta}$ [38] point 1 is valid only for samples with excess of oxygen ($\delta>0$) while for solids with $\delta<0$ the apparent activation energies at HT were higher as compared to those at LT. Point 2 is valid for the system $La_{2-x}Sr_xNiO_{4+\delta}$ studied in [38] and finally, point 3 is valid only for $\delta>0$, while for $\delta<0$ the alternation of the Arrhenius slopes does not happen at a well-defined temperature domain but they change rather gradually and a saddle point appears in the Arrhenius plots [38]. The main reason for the differentiation of the behaviour of the $La_{2-x}Sr_xNi^{2+}_{1-x}Ni^{3+}_xO_{4-\delta}$ and the present system $La_{1-x}Fe^{3+}O_3$ must be the continuous variation of the valence of nickel brought about by the substitution of La^{3+} by the Sr^{2+} cation, details can be found in [16–18,38]. Back to our discussion, with reference to the variation of apparent activation energies (Fig. 8), the picture emerging is summarized in Table 3 for NO and Table 4 for CO.

Table 3
Mechanisms, kinetics and activation parameters for the NO conversion on the $La_{1-x}FeO_3$ solid catalysts

Degree of departure from stoichiometry x in $La_{1-x}FeO_3$	Reaction: $NO_{ads} \rightarrow N_{ads}+O_{ads}$; general reaction rate relationship $R_{NO} = k_{NO}\Theta_{NO} = (k_{NO}K_{NO}P_{NO}/1 + K_{NO}P_{NO} + K_OP_O)$		Conclusions
	Low T	High T	
$LaFeO_3$, $x=0$	$K_{NO}P_{NO}$ large, K_OP_O small $K_{NO}P_{NO} \gg 1+K_OP_O$ $R=k_{NO}$ $E_{app}=E_{true}\approx 60$ kJ/mol	$K_{NO}P_{NO}$ small, K_OP_O small $K_{NO}P_{NO}+K_OP_O \ll 1$ $R=k_{NO}K_{NO}P_{NO}$ $E_{app}=E_{true}-\lambda_{NO}\approx 10$ kJ/mol $\lambda_{NO}\approx 60-10\approx 50$ kJ/mol	λ_{NO} on $LaFeO_3\approx 50$ kJ/mol
$La_{1-x}FeO_3$, $0.35>x>0$ ($La_{0.95}FeO_3$, $x=0.05$)	$K_{NO}P_{NO}$ large, K_OP_O small $K_{NO}P_{NO} \gg 1+K_OP_O$ $R=k_{NO}$ $E_{app}=E_{true}\approx 40$ kJ/mol	$K_{NO}P_{NO}$ small, K_OP_O small $K_{NO}P_{NO}+K_OP_O \ll 1$ $R=k_{NO}K_{NO}P_{NO}$ $E_{app}=E_{true}-\lambda_{NO}\approx 15$ kJ/mol $\lambda_{NO}=40-15\approx 25$ kJ/mol	λ_{NO} on $La_{1-x}FeO_3\approx 25$ kJ/mol
Observations	Difference δE_{true} on $LaFeO_3$ and $La_{1-x}FeO_3$ equals $\approx 60-40\approx 20$ kJ/mol $E_{true}(LaFeO_3)>E_{true}(La_{1-x}FeO_3)$	Difference $\delta\lambda_{NO}$ on $La_{1-x}FeO_3$ and $La_{1-x}FeO_3$ equals $50-25\approx 25$ kJ/mol λ_{NO} $(LaFeO_3)>\lambda_{NO}(La_{1-x}FeO_3)$	

Table 4
Mechanism, kinetics and activation parameters for the CO oxidation on the $La_{1-x}FeO_3$ catalysts

Degree of departure from stoichiometry x in $La_{1-x}FeO_3$	Reaction: $CO_{ads}+O_{ads}\rightarrow CO_{2ads}$, general reaction rate relationship $R_{CO} = k_{CO}\Theta_{CO}\Theta_O = (k_{CO}K_{CO}P_{CO}K_OP_O/(1 + K_OP_O + K_{NO}P_{NO})^2)$		Conclusions
	Low T	High T	
$LaFeO_3$, x=0	$K_{NO}P_{NO}$ large, K_OP_O small $K_{NO}P_{NO} \gg 1+K_OP_O$ $R = (k_{CO}K_{CO}P_{CO}K_OP_O)/(K_{NO}P_{NO})^2$, $E_{app}=E_{true}-\lambda_{CO}-\lambda_O+2\lambda_{NO}\approx 110$ kJ/mol	$K_{NO}P_{NO}$ small, K_OP_O small $K_{NO}P_{NO}+K_OP_O \ll 1$ $R=k_{CO}K_{CO}P_{CO}K_OP_O$ $E_{app}=E_{true}-\lambda_{CO}-\lambda_O$ ≈ 20 kJ/mol	λ_{NO} on $LaFeO_3\approx 45$ kJ/mol
$La_{1-x}FeO_3$, $0.35>x>0$ ($La_{0.95}FeO_3$, x=0.05)	$K_{NO}P_{NO}$ large, K_OP_O small $K_{NO}P_{NO} \gg 1+K_OP_O$ $R = (k_{CO}K_{CO}P_{CO}K_OP_O)/(K_{NO}P_{NO})^2$ $E_{app}=E_{true}-\lambda_{CO}-\lambda_O+2\lambda_{NO}$ ≈ 40 kJ/mol	$K_{NO}P_{NO}$ small, K_OP_O small $K_{NO}P_{NO}+K_OP_O \ll 1$ $R=k_{CO}K_{CO}P_{CO}K_OP_O$ $E_{app}=E_{true}-\lambda_{CO}-\lambda_O$ ≈ 15 kJ/mol	λ_{NO} on $La_{1-x}FeO_3\approx 25$ kJ/mol
Observations	Difference δE_{app} on $LaFeO_3$ and $La_{1-x}FeO_3$ equals$\approx$110−40 $\approx$70 kJ/mol $E_{app}(LaFeO_3)>E_{app}(La_{1-x}FeO_3)$	Difference $\delta\lambda_{NO}$ on $LaFeO_3$ and $La_{1-x}FeO_3$ equals 45−25 $\approx$20 kJ/mol λ_{NO} ($LaFeO_3$)>λ_{NO} ($La_{1-x}FeO_3$)	

4.3. Mechanism for the NO conversion

Let us discuss first Table 3 which contains all the mechanistic aspects of NO conversion, including kinetics and the activation parameter found experimentally. Briefly the data existing in this table can be described as follows: The slow and rate determining step for the NO conversion is the dissociation of NO_{ads} to O_{ads} and N_{ads} [1,3,9,29,43–45]

$$NO_{ads} \rightarrow N_{ads} + O_{ads} \quad (3)$$

The corresponding Langmuir reaction rate describing the step is

$$R_{NO} = k_{NO}\Theta_{NO} = \frac{k_{NO}K_{NO}P_{NO}}{1 + K_{NO}P_{NO} + K_OP_O}, \quad (4)$$

where the symbols have their usual meaning. The samples $La_{1-x}FeO_3$ are differentiated into two classes according to the activation parameters determined on them (see Fig. 8): Only the sample $LaFeO_3$ (x=0) belongs to the first class (I), while to the second class (II) belong all the samples $La_{1-x}FeO_3$ ($0.35\geq x>0.0$) whose behaviour was somehow similar.

Each class is differentiated by its behaviour at LT and HT.

(i) *Class I – $LaFeO_3$ at LT.* In this case $K_{NO}P_{NO}$ is large but K_OP_O is small and $R_{NO}=k_{NO}$. Therefore $E_{app}(NO, LT)\approx E_{true}(NO, LT)\approx 60$ kJ/mol.

(ii) *Class II – $La_{1-x}FeO_3$ at LT.* Again $K_{NO}P_{NO}$ is large and K_OP_O is small, $R_{NO}=k_{NO}$ and $E_{app}(NO, LT)\approx 40$ kJ/mol.

(iii) *Class I – $LaFeO_3$ at HT.* Here $K_{NO}P_{NO}$ and K_OP_O are small and $R_{NO}=k_{NO}K_{NO}P_{NO}$. Therefore $E_{app}(NO, HT)=E_{true}(NO, HT)-\lambda_{NO}\approx 10$ kJ/mol. Accepting that on the $LaFeO_3$ solid $E_{true}(NO, HT)=E_{true}(NO, LT)\approx 60$ kJ/mol (see (i)), then $\lambda_{NO}(LaFeO_3)\approx 50$ kJ/mol.

(iv) *Class II – $La_{1-x}FeO_3$ at HT.* Again $K_{NO}P_{NO}$ and K_OP_O are small, $R_{NO}=k_{NO}K_{NO}P_{NO}$ and $E_{app}(NO, HT)=E_{true}(NO, HT)-\lambda_{NO}\approx 15$ kJ/mol. Accepting that on $La_{1-x}FeO_3$ solids $E_{true}(NO, HT)=E_{true}(NO, LT)\approx 40$ kJ/mol (see (ii)), then $\lambda_{NO}(La_{1-x}FeO_3)=25$ kJ/mol.

The conclusions from points (i)–(iv) are as follows:

Points (i) and (ii). The difference between the true activation energies on the solids $LaFeO_3$ and $La_{1-x}FeO_3$ equals around 20 kJ/mol. The lower values of E_{true} on the second set of solids $La_{1-x}FeO_3$ results in their increased activity.

Points (iii) and (iv). The difference between the heats of adsorption of NO on the solid $LaFeO_3$ and $La_{1-x}FeO_3$ equals around 25 kJ/mol. The $LaFeO_3$ solid seems to adsorb stronger than the NO. It is worthwhile to mention here that the true activation energy in the $LaFeO_3$ appears higher by an amount of ~25 kJ/mol as compared to $La_{1-x}FeO_3$ solid, which almost matches the higher value of λ_{NO} (~20 kJ/mol) estimated for the $LaFeO_3$ sample as compared to $La_{1-x}FeO_3$ solids.

4.4. Mechanism of CO reaction

Let us now discuss the data for the CO reaction towards CO_2 included in Table 4. This table contains again possible kinetics and activation parameters found experimentally. The slow and rate determining step is the reaction between the CO_{ads} and O_{ads} towards CO_2 [1,3,9,29,43–45]

$$CO_{ads} + O_{ads} \rightarrow CO_{2ads} \quad (5)$$

which is subsequently desorbed. The reaction rate is given by the equation

$$R_{CO} = k_{CO}\Theta_{CO}\Theta_O = \frac{k_{CO}K_{CO}P_{CO}K_OP_O}{(1+K_OP_O+K_{CO}P_{CO}+K_{CO_2}P_{CO_2}+K_{NO}P_{NO})^2}. \quad (6)$$

Then considering that CO and CO_2 are more weakly adsorbed on the surface as compared to oxygen and NO we arrive at the simplified relation

$$R_{CO} = \frac{k_{CO}K_{CO}P_{CO}K_OP_O}{(1+K_OP_O+K_{NO}P_{NO})^2}. \quad (7)$$

We shall differentiate now the discussion for the low temperature (LT) and high temperature (HT) region as well as for the $LaFeO_3$ and $La_{1-x}FeO_3$ solids which showed differentiated behaviour (see Table 1 and Fig. 5). We draw also attention to the fact that the assumptions made next are exactly the same as those made for the NO conversion (see Table 3).

(i) *Class I – $LaFeO_3$ at LT*. In this case $K_{NO}P_{NO}$ is large but K_OP_O is small and $R_{CO}=k_{CO}K_{CO}P_{CO}K_O/(K_{NO}P_{NO})^2$. Therefore $E_{app}(CO, LT)=E_{true}(CO, LT)-\lambda_{CO}-\lambda_O+2\lambda_{NO}\approx 110$ kJ/mol.

(ii) *Class II – $La_{1-x}FeO_3$ at LT*. The same as above and $E_{app}(CO, LT)\approx E_{true}(CO, LT)-\lambda_{CO}-\lambda_O+2\lambda_{NO}\approx 40$ kJ/mol.

(iii) *Class I – $LaFeO_3$ at HT*. Here $K_{NO}P_{NO}$ and K_OP_O are both small and $R_{CO}=k_{CO}K_{CO}P_{CO}K_OP_O$. Therefore, $E_{app}(CO, HT)=E_{true}(CO, HT)-\lambda_{CO}-\lambda_O\approx 20$ kJ/mol. Accepting that on the $LaFeO_3$ solid $E_{true}(CO, LT)-\lambda_{CO}-\lambda_O\approx E_{true}(CO, HT)-\lambda_{CO}-\lambda_O$, in other words, that the heats of adsorption λ_i as well as the true activation energies are similar at LT and HT, then $\lambda_{NO}(LaFeO_3)\approx 45$ kJ/mol. This result is in very good agreement with the corresponding values of $\lambda_{NO}\approx 50$ kJ/mol calculated in Table 3 from the NO data.

(iv) *Class II – $La_{1-x}FeO_3$ at HT*. The same as in (iii) above and $E_{app}(CO, HT)=E_{true}(CO, HT)-\lambda_{CO}-\lambda_O\approx 15$ kJ/mol. Accepting again that the E_{true} and λ_i values are similar on the $La_{1-x}FeO_3$ solids, then $\lambda_{NO}(La_{1-x}FeO_3)\approx 15$ kJ/mol. The corresponding value from the data of NO was found to be around ~25 kJ/mol. The conclusions from points (i)–(iv) are as follows:

Points (i) and (ii). The difference between the apparent activation energies on $LaFeO_3$ and $La_{1-x}FeO_3$ solids is around 70 kJ/mol. The higher apparent activation barrier in the $LaFeO_3$ solid results in decreased activity.

Points (iii) and (iv). The difference between the heats of adsorption on the $LaFeO_3$ and $La_{1-x}FeO_3$ solids equal around 20 kJ/mol. This result is in good agreement indeed with the conclusions made in Tables 3 and 4. It is precisely such internal agreements of the data which make us believe that the proposed model reflects indeed the reality.

4.5. Production and elimination of N_2O

During the reaction course some N_2O is produced especially at low temperatures. The amount of N_2O produced vs. temperature is shown in Fig. 4 as a function of difference $X_{NO}-X_{CO}$ as well as in Fig. 5 as a function of the parameter x of the $La_{1-x}FeO_3$ solids. We observe in Fig. 4 that the variation of N_2O with temperature reaches a maximum which depends on the catalysts. This production of N_2O is well known and proceeds via the following reactions:

$$NO_g \rightarrow NO_{ads} \quad (8)$$

$$NO_{ads} \rightarrow N_{ads} + O_{ads} \quad (9)$$

$$N_{ads} + NO_{ads} \rightarrow N_2O_{ads} \quad (10)$$

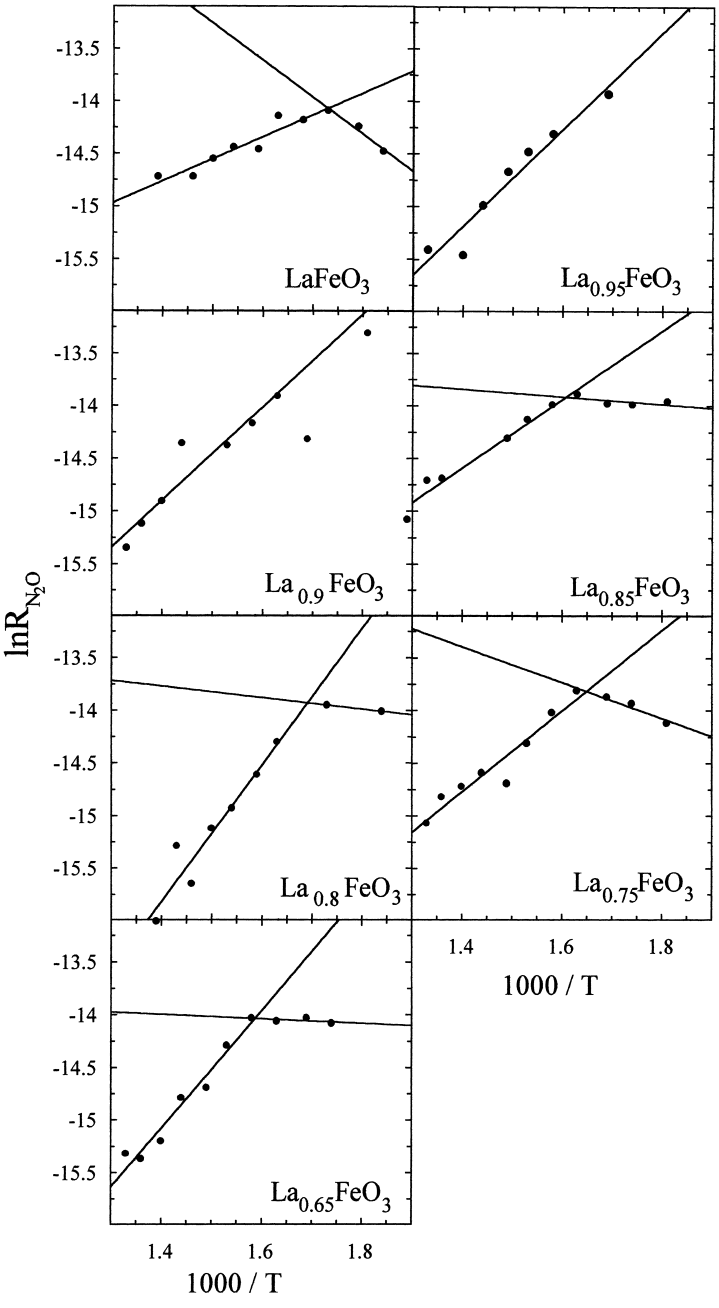

Fig. 9. Arrhenius plots for the N_2O conversion.

$$N_2O_{ads} \rightarrow N_2O_g \quad (11)$$

The critical step is the NO_{ads} scission (reaction (9)) producing enough N_{ads} to fuel step (10). The depletion of N_2O can be either due to its decomposition towards N_2 and O_2 or to depletion of N_{ads} from the surface:

$$N_2O_{ads} \rightarrow N_{2g} + O_{ads} \quad (12)$$

$$2N_{ads} \rightarrow N_{2g} \quad (13)$$

Now the decomposition of N_2O itself takes place at higher temperatures as compared to NO+CO conversion as can be seen by a comparison of the data in [16] and [43]. Therefore we consider that the nitrogen desorption (reaction (13)) is actually the reason for the drop of N_2O production as temperature increases. In order to estimate the energetic parameters of the N_2O formation and elimination we have plotted in Fig. 9 plots of the form log-($N_2O_{arbitr.units}$) vs. 1000/T.

The calculated values of activation parameters are noticed in Table 1. Of them the values found at low temperatures are of *kinetic origin* while the values at high temperatures are of *thermodynamic origin*. To be more precise, considering that reaction (9) is the controlling step for the N_2O formation then

$$R_{N_2O} = R_{NO_{ads.scission}} = k\theta_{NO_{ads}} = kK_{NO}P_{NO} \quad (14)$$

and therefore

$$E_{app.\,N_2O\ formation} = E_{true} - \lambda_{NO}, \quad (15)$$

where λ_{NO} is the heat of adsorption of NO. The values of $E_{app.\,N_2O}$ tend to zero for $x>0$ in $La_{1-x}FeO_3$, except when $x=0.25$. Therefore in these cases $E_{true}\approx\lambda_{NO}$. For the sample $LaFeO_3$, $E_{app.}=29.2$ kJ/mol which means that NO is more weakly adsorbed in its surface by almost 25–30 kJ/mol, on the average, as compared to the $La_{1-x}FeO_3$ ($x>0$) solids. This is in good agreement with the difference of λ_{NO} values for the two group of samples calculated in Tables 3 and 4. The drop in the N_2O production as temperature increases (see Fig. 4) is due, according to the above, to the depletion of surface from N_{ads} according to reaction (10). Therefore the negative ''activation'' energies found (see Table 1) are referred to the heats of desorption of N_2 from the perovskite surface which is around 38±10 kJ/mol on $La_{1-x}FeO_3$ ($x>0$) solids but only ~10 kJ/mol for $LaFeO_3$. In other words the N_{ads} is rather weakly adsorbed (~10 kJ/mol) on the $LaFeO_3$ but more strongly adsorbed on the $La_{1-x}FeO_3$ ($x=0.05$–0.35) solids. We remind that the heat of adsorption of nitrogen on doubly promoted reduced iron has been found to be between 10 ($\theta\rightarrow1$) and 45 kJ/mol ($\theta\rightarrow0$) depending on the surface coverage [46] so that the values found here are in the correct order of magnitude for similar systems.

5. Conclusions

The solids of the general formula $La_{1-x}FeO_3$ ($LaFeO_3$ at $x\leq0.05$, $LaFeO_3+Fe_2O_3$ at $x>0.05$) are more active catalysts for the NO+CO reaction at $x>0$ than $LaFeO_3$. The solid particles for $0.35\geq x>0.00$ seem to possess an outer shell composition around $La_{0.95}FeO_3$ while the excess of iron oxide forms a core in the inside of the particles. The conversion of NO via decomposition to nitrogen and oxygen as well as the oxidation of CO by the oxygen produced via the scission of NO are differentiated at the low and high temperature regions, exhibiting distinctively lower apparent activation energies (E_{app}) at high temperatures but higher E_{app} at low temperatures. This differentiation is controlled by the kinetics of the heterogeneous reaction which is in turn controlled by the relative heats of adsorption of NO and the oxygen on the surface. The heats of adsorption of NO on the $LaFeO_3$ and $La_{1-x}FeO_3$ solids have been calculated. The deviation from stoichiometry up to $x=0.05$, as well as the heating of the solids during preparation under vacuum, favours the catalytic action. On the contrary, the stoichiometric solid $LaFeO_3$ is less active, while heating of the catalysts under atmospheric conditions diminishes their activity appreciably.

References

[1] B.K. Cho, B.H. Shanks, J.E. Bailey, J. Catal. 115 (1989) 489.
[2] B.K. Cho, J. Catal. 138 (1992) 255.
[3] R.W. McCabe, C. Wong, J. Catal. 121 (1990) 422.
[4] B.A. Banse, D.T. Wickham, B.E. Koel, J. Catal. 119 (1989) 238.
[5] S.H. Oh, J. Catal. 124 (1990) 477.
[6] S.H. Oh, C.C. Eickel, J. Catal. 128 (1991) 526.
[7] B.K. Cho, J. Catal. 131 (1991) 74.
[8] D.R. Rainer, S.M. Vesecky, M. Koranne, W.S. Oh, D.W. Goodman, J. Catal. 167 (1997) 234.
[9] W.C. Hecker, A.T. Bell, J. Catal. 84 (1983) 200.
[10] E. Novak, D. Sprinceana, F. Solymosi, Appl. Catal. A 149 (1997) 89.
[11] A. Kudo, M. Steinberg, A.J. Bard, A. Campion, M.A. Fox, T.E. Mallouk, S.E. Webber, J.M. White, J. Catal. 125 (1990) 565.
[12] J. Barton, Collect. Czech. Chem. Commun. 55 (1990) 1935.
[13] N. Mizuno, Y. Fujiwara, M. Misono, J. Chem. Soc., Chem. Commun. 3 (1989) 316.
[14] A.M. Olivan, M.A. Pena, L.G. Tejuca, J.M.D. Tascon, J. Mol. Catal. 45 (1988) 355.

[15] J.M.D. Tascon, L.G. Tejuca, C.H. Rochester, J. Catal. 95 (1985) 558.
[16] A.K. Ladavos, P.J. Pomonis, Appl. Catal. B 1 (1992) 101.
[17] A.K. Ladavos, P.J. Pomonis, Appl. Catal. B 2 (1993) 27.
[18] A.K. Ladavos, P.J. Pomonis, Catal. Today 17 (1993) 181.
[19] Y. Teraoka, H. Nii, S. Kagawa, K. Jahnsson, M. Nygren, J. Mater. Chem. 6(1) (1996) 97.
[20] O. Inoue, S. Kawashima, Eur. Patent 0 237 081 (1987).
[21] H. Tanaka, S. Matsumoto, H. Sobukawa, M. Ozawa, Eur. Patent 0 525 677 (1992).
[22] S. Sekido, H. Tachibana, Y. Ninomiya, Eur. Patent 0 089 199 (1983).
[23] A. Lindstedt, D. Stroemberg, M. Abul Milh, Appl. Catal. A 116 (1994) 109.
[24] M. Ocal, R. Oukaci, G. Marcelin, S.K. Agarwal, Ind. Eng. Chem. Res. 33 (1994) 2930.
[25] T. Nitadori, S. Kurihara, M. Misono, J. Catal. 98 (1986) 221.
[26] T. Nitadori, M. Misono, J. Catal. 93 (1985) 459.
[27] N. Mizuno, M. Tanaka, M. Misono, J. Chem. Soc., Faraday Trans. 88 (1992) 91.
[28] L. Shi-Yao, L. Bei-Lu, React. Kinet. Catal. Lett. 57 (1996) 183.
[29] R.J.H. Voorhoeve, J.P. Remeika, L.E. Trimble, Ann. NY Acad. Sci. 272 (1976) 3.
[30] J.M.G. Amores, V.S. Escribano, M. Daturi, G. Busca, J. Mater. Chem. 6 (1996) 879.
[31] G. Longworth, in: G.J. Long (Ed.), Moessbauer Spectroscopy Applied to Inorganic Chemistry, vol. I, Plenum Press, New York, 1984, p. 43.
[32] M. Eibschutz, S. Shtrikman, D. Treves, Phys. Rev. 2 (1967) 562.
[33] H.M. Rietveld, Acta Cryst. 22 (1967) 151.
[34] H.M. Rietveld, J. Appl. Cryst. 2 (1969) 65.
[35] D.B. Wiles, R.A. Young, J. Appl. Cryst. 14 (1981) 149.
[36] D.L. Bish, S.A. Howard, J. Appl. Cryst. 21 (1988) 86.
[37] R.W.G. Wyckoff, Crystal Structures, vols. 2 and 3, Interscience, London, 1964.
[38] A.K. Ladavos, P.J. Pomonis, Appl. Catal. A 165 (1997) 73.
[39] L. Simonot, F. Garin, G. Maire, Appl. Catal. 11 (1997) 181.
[40] K.C. Taylor, Catal. Rev.-Sci. Eng. 35(4) (1993) 457.
[41] B. Viswanathan, Catal. Rev.-Sci. Eng. 34(4) (1992) 337.
[42] N. Mizuno, M. Yamato, M. Misono, J. Chem. Soc., Chem. Commun. (1988) 887.
[43] A.K. Ladavos, P.J. Pomonis, J. Chem. Soc., Faraday Trans. 87 (1991) 3291.
[44] R.J.H. Voorhoeve, in: J.J. Burton, R.L. Garten (Eds.), Advanced Materials in Catalysis, Academic Press, New York, 1977, p. 129.
[45] R.J.H. Voorhoeve, J.P. Remeika, L.E. Trimble, in: R.L. Klimisch, J.G. Larson (Eds.), The Catalytic Chemistry of Nitrogen Oxides, Plenum Press, New York, 1975, p. 215.
[46] K. Tamaru, Dynamic Heterogeneous Catalysis, Academic Press, London, 1978, p. 68.